ACS Sustainable Chemistry & Engineering

pubs.acs.org/journal/ascecg

Research Article

Coprecipitation of Crystalline Calcium Silicates and Carbonates from the Hydrothermal Reaction of Pseudowollastonite

Coleman Tolliver, Suzanne Nguyen, Kimmie Dela Cerna, Rachel McNamara, Elizabeth J. Opila, and Andres F. Clarens*

Cite This: *ACS Sustainable Chem. Eng.* 2024, 12, 1844−1856

Read Online

ABSTRACT: Calcium silicates are abundant but sparingly soluble feedstocks of interest for making low-carbon alternative cements. Under hydrothermal and alkaline conditions, they can form crystalline calcium silicate hydrate (CCSH) products, which are abundant in Roman concrete, or they can form carbonates when CO_2 is present. To understand when coprecipitation of CCSH and carbonate phases is possible, we studied the hydrothermal carbonation of a model calcium silicate, pseudowollastonite (α-$CaSiO_3$), at 150 °C and high pH as a function of CO_2 source [CO_2(g) or Na_2CO_3] and different concentrations of sodium, alumina, and silica. Our experiments produced a range of CCSH phases including tobermorite−13 Å, rhodesite, and pectolite, as early as 1 day after the start of our experiments. After 7 days of curing in a 2 M NaOH solution, over 10% of the samples had been converted to these CCSH phases. We also observed the formation of $CaCO_3$ as both aragonite and calcite when carbon was introduced to our experimental system. The carbon source impacted the ratio of the $CaCO_3$ to CCSH phases in the reaction products. The availability of Na_2CO_3 produced a balance between the $CaCO_3$ and CCSH phases, whereas CO_2(g) produced more $CaCO_3$, with samples that were over one-third carbonate by mass. Higher concentrations of Na^+ increased the precipitation of both the $CaCO_3$ and CCSH phases. The presence of excess silica, in the form of dissolved borosilicate glass from our reaction vessels under alkaline reaction conditions, also enhanced the formation of CCSH phases formed in some experiments. Supplemental Al_2O_3, a common constituent in many silicate feedstocks, also enhanced CCSH formation, likely by forming aluminum-substituted phases under the conditions tested here. These chemical insights can enable the design of formulation and curing guidelines for novel cementitious materials.

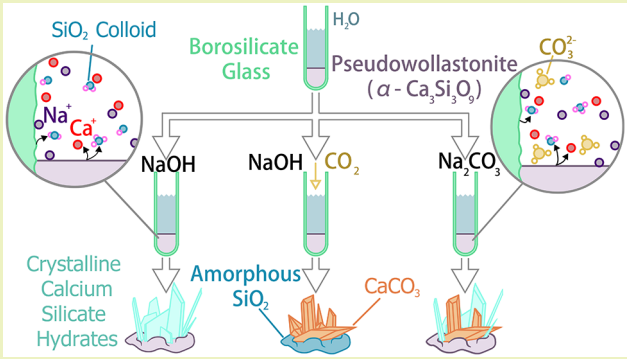

KEYWORDS: *low carbon cement, monocalcium silicate, tobermorite, curing, carbonation*

■ INTRODUCTION

The global cement industry produces nearly 8% of annual CO_2 emissions, and these emissions are expected to increase as more nations continue to develop their infrastructure.[1] Ordinary Portland Cement (OPC), the most common cement, is made by calcining, that is, decomposing at high temperatures, $CaCO_3$ from limestone into CaO and CO_2(g). The emission intensity is driven, in part, by the direct emissions of this CO_2 and, in part, by the fossil fuels needed to heat the kilns to 1450 °C.[2] With global demand for cement topping 4 billion metric tons in 2022,[3] the industry is seeking alternatives that can be produced with lower emissions at large scale and at low cost.

Alternative cementitious materials sourced from reactants that do not require CaO from $CaCO_3$ decomposition and that are able to sequester CO_2 could provide a decarbonation pathway for the cement industry.[4] Slags from ore refinement or metal manufacturing and ashes from combustion are widely abundant and underutilized resources in the cement industry.[5] A large body of literature explores mix designs and curing techniques that incorporate waste slags and ashes to further improve OPC hydration.[6−9] The waste products can improve the compressive strength and other properties by increasing the formation of calcium silicate hydrate (CSH) gel, the key reaction product of OPC hydration.[10] These materials are rich in calcium silicates, which are generally not hydraulically activated, like OPC, but they can be reacted to form cementitious materials on their own using alkali or temperature activation.[11−13] As one example, the calcium silicate pseudowollastonite (α-$CaSiO_3$) can be carbonated in alkaline conditions and elevated temper-

Received: August 11, 2023
Revised: December 22, 2023
Accepted: December 27, 2023
Published: January 25, 2024

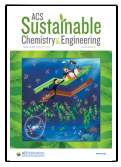

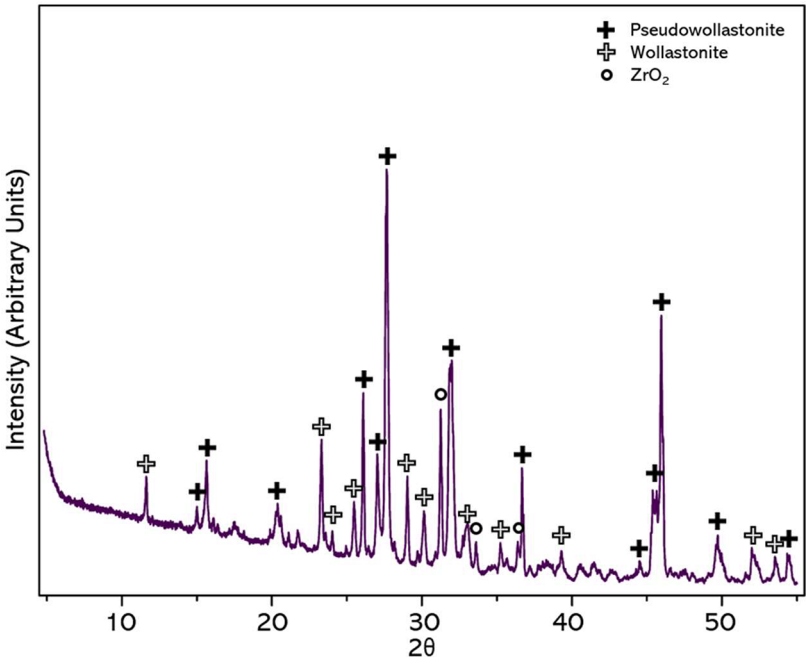

Figure 1. XRD pattern of the synthesized pseudowollastonite. Some peaks corresponding to wollastonite ($CaSiO_3$, low-temperature polymorph) were present. Our feedstock was estimated to contain 70% pseudowollastonite using Rietveld refinement via *GSAS-II*.[39]

atures to produce crystalline calcium silicate hydrate (CCSH) phases alongside calcium carbonates.[14−17]

CCSH phases, like tobermorite−11 Å [$Ca_4Si_6O_{16}(OH)_2 \cdot 4H_2O$], are not abundant in conventional OPC mortars or concretes because they generally only form at higher temperatures between 80 and 180 °C.[18] Nevertheless, CCSH phases are desirable in concrete because of the strengths they provide relative to the CSH gel. Ancient Roman concretes, for example, have been found to contain aluminum-substituted tobermorite−11 Å (Al-tobermorite), which contributes to their strength and durability.[19−22] Ancient Roman concretes are thought to have cured at elevated temperatures as a result of the reaction of lime with seawater to form portlandite [$Ca(OH)_2$], with temperatures estimated to reach up to 97 °C.[19] The portlandite reacted with volcanic ashes to form a calcium aluminum silicate hydrate gel, which then crystallized into Al-tobermorite and other ordered phases over time. Another key feature of Roman concrete is its high porosity,[21] which allowed seawater to slowly dissolve glass aggregates. The resulting alkali- and silica-rich pore solution further facilitated the growth of Al-tobermorite over centuries.[21]

The tobermorite synthesis literature generally reports on mixtures of CaO and a finely ground SiO_2 source, like quartz or amorphous SiO_2, combined at a Ca:Si molar ratio of 5:6 to match the stoichiometry of tobermorite.[18,23−29] The powders are then cured hydrothermally at temperatures over 80 °C for days to weeks.[18,23−29] Tobermorite formation is thought to result from the crystallization of CSH gel initially formed when CaO, SiO_2, and H_2O react.[23−29] Tobermorite synthesis has also been studied with additives like NaOH and Al_2O_3.[23,25−28,30,31] NaOH has been shown to hinder the crystallization of tobermorite during synthesis by stabilizing the CSH gel formed.[28,32] Here crystallinity refers to the diffraction intensity observed, indicative of the ordering that the system has undergone. Trace amounts of aluminum have also been shown to impact the crystallization of tobermorite, but the mechanism is complex. Matekonis,[28] Mitsuda,[32] Guo,[23] and Shaw[29] all reported increases in tobermorite precipitation in the presence of Al_2O_3, whereas Gabrovsek[25] and Maeda[27] reported decreases in tobermorite crystallinity in the presence of Al_2O_3. Matekonis and Cao suggested a positive correlation between NaOH, Al_2O_3 and tobermorite crystallinity.[28,33]

Research exploring tobermorite synthesis from calcium silicates and calcium aluminum silicates has demonstrated that alkaline solutions are required for precipitation.[16,17,34,35] Sodium bases, such as NaOH, have been shown to facilitate the precipitation of tobermorite better than other alkali metals.[17,35] Tobermorite precipitation from calcium silicates has also been described as the crystallization of CSH gel.[17,34−36] The formation of tobermorite and other CCSH phases from pseudowollastonite has been shown to increase when exposed to both sodium and CO_2; CCSH phases have precipitated when the carbon is delivered as a salt, for example, as Na_2CO_3 or $NaHCO_3$[17] or CO_2 gas and NaOH.[14−16] However, the effects of CO_2 and sodium concentrations on the amount and phases of precipitated CCSH have not been explored in detail. Prior work in our laboratory suggested that the crystal structure and dissolution characteristics of the parent silicate were a major factor impacting CCSH precipitation.[14] Pseudowollastonite has three-membered silicate rings in its crystal structure that result in congruent dissolution, unlike the silicate chains in wollastonite (low-temperature polymorph of $CaSiO_3$), which result in congruent dissolution.[37] The higher concentration of aqueous silica in solution from pseudowollastonite dissolution could facilitate CCSH precipitation after the system is saturated with calcium carbonates.[14]

To better characterize the ways in which the CCSH phases form during the carbonation of calcium silicates, we explore the reaction of pseudowollastonite under hydrothermal conditions with CO_2. First, we sought to understand the effect of independently varying the partial pressure of CO_2 (or $NaCO_2$ concentration) and NaOH concentrations on pseudowollastonite carbonation. Second, the experiments were conducted in the presence of borosilicate glass to understand how dissolution

https://doi.org/10.1021/acssuschemeng.3c05110
ACS Sustainable Chem. Eng. 2024, 12, 1844−1856

of this silica source would impact the reactions, as it did in Roman concretes. Third, we explored the presence and absence of Al_2O_3 on CCSH precipitation.

MATERIALS AND METHODS

Materials. Pseudowollastonite was synthesized from a 0.95:1 molar ratio of $CaCO_3$ (Huber, 97% pure) and Elkem micro silica 965 (95% pure), respectively. The powders were combined and then ball-milled for 1 h. The powder was then placed in a bowl and weighed. A 1.25 M NaOH (Fisher, 97% pure) solution, at a mass of 25% of the combined powders, was mixed in using a KitchenAid Classic 4.5 L mixer. The slurry was baked into a solid slab at 80 °C for 24 h. The slab was fired to 1250 °C, above the 1125 °C transformation temperature of wollastonite (β-$CaSiO_3$) to pseudowollastonite,[38] and held at that temperature for 9 h in an Evenheat 1818 HF II pottery kiln. A section of the fired material was broken off and ground for powder X-ray diffraction (XRD; Malvern-Panalytical Empyrean, Worcestershire, U.K.). When confirmed to be pseudowollastonite, the fired material was broken with a hammer and chisel and ground via a hand mill into a coarse powder. The powder was then ball-milled using ZrO_2 media for 24 h and filtered through a #200 sieve (75 μm). The separated powder was ball-milled again for 24 h before being stored in a sealed container. Figure 1 shows the XRD pattern of the synthesized pseudowollastonite. Wollastonite is present, and ZrO_2 is an impurity from the milling media. Rietveld analysis using *GSAS-II*[39] indicates that about 70% by mass was pseudowollastonite and up to 20% was wollastonite and ZrO_2, rankinite ($Ca_3Si_2O_7$), and calcio-olivine (Ca_2SiO_4) were all ≤3%.

Hydrothermal Experiments. A feedstock, either 2 g of pseudowollastonite or 1.9 g of pseudowollastonite + 0.1 g of α-Al_2O_3 (Fisher, 99.9% pure), was placed in a 25 mL borosilicate test tube (Fisher 14-962-26K) and filled with 20 mL of either deionized (DI) water or a 1 or 2 M NaOH solution. The test tubes were placed in a rack and sealed in a 10 L pressure vessel with 2 L of water in the base. CO_2 was injected via a syringe pump and allowed to equilibrate for 1 h to attain P_{CO_2} values of 3, 6, 15, or 30 psi at 150 °C. The syringe pump has an accuracy of ±1 psi. The vessels were then heated in an oven at 150 °C (±3 °C) in accordance with prior work[14,17,26] for 1, 3, or 7 days of curing. Experiments without gaseous CO_2 were conducted in a completely isolated pressure vessel. Experiments using Na_2CO_3 (Fisher, 99.5% pure) with sodium concentrations at 1 or 2 M were also conducted in an isolated pressure vessel at a P_{CO_2} value of 0 psi and the same temperature and times. Table 1 lists the experimental factors and the number of levels for each factor. The vessels were removed from the oven, and the test tubes were naturally cooled to room temperature after the desired cure time. The precipitates were filtered from solution using 25 μm filter paper (Whatman), acidified with 0.1 M acetic acid (Fisher, glacial), then dried at 50 °C for 24 h, and stored. Additional borosilicate test tubes were filled with 20 mL of DI water and 1 or 2 M NaOH and exposed to the same hydrothermal conditions and times without reactant powder.

Table 1. Experimental Conditions Tested Here[a]

Na^+ source	$[Na^+]$ (M)	time (days)	P_{CO_2} (psi)	Al_2O_3 (%)
NaOH	0	1	0	0
Na_2CO_3	1	3	3	5
	2	7	6	
			15	

[a]These variables were combined across all levels listed here.

Characterization. Powder XRD of the dried precipitates was conducted with the following parameters: Cu Kα radiation (λ = 1.5405 Å), current = 40 mA, tension = 45 kV, GaliPIX detector scanning 501 steps at a time, measurement range 2θ = 4.8−55°, time per step = 90 s, and step size 2θ = 0.0143°. The sample stage was spun during the scans to minimize the effects of orientation. The data were analyzed with *Highscore Plus* (version 4.9) using the International Centre for Diffraction Data (ICDD) database to identify phases. Table 2 contains the mineral names, compositions, and ICDD reference codes of the phases identified in this work. All patterns of the major (>10% mass) and minor (2−10%) phases identified showed good agreement of their peak locations and intensities with the reference data.

Select samples were further analyzed via thermogravimetric analysis (TG; Netzsch STA-449 F1, München, Germany) to quantify the amount of hydration and carbonation. For this characterization, 20 mg of powder was placed in a Pt−Rh crucible and heated at a rate of 10 °C/min to 1000 °C. The data were collected and compared to those in the literature.[40−42] Supernatants from the powderless glass experiments were analyzed via inductively coupled plasma optical emission spectroscopy (ICP-OES, Thermofisher ICAP 6200, Waltham, MA). The supernatants were diluted to 2000× with DI water. Standards Al, B, Ca, K, Na, and Si (Inorganic Ventures) were used for calibration. Supernatant concentrations were measured in triplicate.

Attempts were made to characterize individual powders using single-crystal XRD (Bruker APEXII diffractometer, Billerica, MA) and transmission electron microscopy (FEI Titan 80-300). However, reaction products contained crystals too small to get usable data from and too numerous to select representative phases of interest.

RESULTS

Reactions with NaOH. When reacted in the presence of concentrated base (2 M NaOH) at a temperature of 150 °C, pseudowollastonite forms a range of CCSH phases including tobermorite−13 Å, pectolite, and rhodesite, as shown in the XRD patterns in Figure 2a. Our feedstock contained both pseudowollastonite and wollastonite, and both declined in intensity with time as they were consumed to form CCSH phases. The amount of CCSH produced increased with time. Pectolite was the first phase to form, with small peaks seen after 1 day. Rhodesite contained some potassium, which most likely came from dissolution of the glass vials used as curing vessels. A broad peak at approximately 2θ = 7.3° was present in the XRD patterns, which may correspond to poorly crystalline tobermorite−11 Å or rhodesite. Prominent peaks for both tobermorite−13 Å and rhodesite were seen clearly after 3 days. In addition to CCSH phases, we also observed the formation of a sodium aluminum silicate phase, referred to as gismondine-Na, after 1 day. The aluminum needed for gismondine-Na to form also likely came from borosilicate glass dissolution.

The derivative of the TG (differential thermal gravimetry, DTG) data after 1 day (Figure 2b) showed appreciable dehydration, indicative of water bound in the CSH gel, corresponding to the DTG peak at about 90 °C.[40] Structurally bound water in pectolite and gismondine-Na was also expected to contribute to this dehydration peak. In the 3 day samples where CCSH phases formed, tobermorite −13 Å was expected to dehydrate into tobermorite−11 Å in the same temperature range as CSH gel dehydration,[43] increasing the peak at 90 °C. The peak found at 175 °C corresponds to tobermorite−11 Å dehydration,[43] while the peak at 250 °C is attributed to rhodesite and gismondine-Na dehydration. For the 7 day sample, water lost to dehydration of the CCSH phases accounted for 10.7% of the total mass, indicating that CCSH phases comprised a significant amount of the sample. It is also worth noting that pseudowollastonite was not completely converted to reaction products under the conditions tested here.

Reactions with NaOH and Variable P_{CO_2}. The addition of CO_2 resulted in the formation of the calcium carbonates aragonite and calcite and less CCSH phases across all P_{CO_2} conditions, especially at the highest P_{CO_2} levels tested, as seen in Figure 3. The data presented in Figure 3 were collected from

https://doi.org/10.1021/acssuschemeng.3c05110
ACS Sustainable Chem. Eng. 2024, 12, 1844−1856

Table 2. List of Mineral Names, Chemical Formulas, and ICCD Reference Codes for the Phases Identified in This Work[a]

mineral name	chemical formula	ICDD reference code
pseudowollastonite (+)	$CaSiO_3$	01-080-9543
wollastonite (+)	$CaSiO_3$	02-027-1064
aragonite (−)	$CaCO_3$	04-013-9616
calcite (−)	$CaCO_3$	04-008-0198
α-Al_2O_3 (−)	Al_2O_3	00-005-0712
zirconia (t)	ZrO_2	04-013-4749
tobermorite−13 Å (+)	$Ca_{16}(Si_8O_{28})(H_2O)_{13}$	01-081-9793
pectolite (−)	$NaCa_2Si_3(OH)$	01-076-0951
rhodesite (+)	$(Ca,K,Na)_8Si_{16}O_{40}\cdot 11H_2O$	00−022-1253
unnamed CCSH (−)	$Ca_9(Si_{16}O_{34}(OH)_{14})(H_2O)_8$	01-074-7587
gismondine-Na (−)	$Na_{3.6}Al_{3.6}Si_{12.4}O_{32}\cdot 14H_2O$	01-080-0699
analcime (−)	$K_{0.19}Na_{7.69}Ca_{0.06}Al_8Si_{16}O_{48}(H_2O)_8$	04-024-8347

[a]Major phases over an estimated 10% mass are indicated by (), minor phases from 2 to 10% mass by (−), and trace phases under 2% by (t).

samples cured in 2 M NaOH for a comparison to the results presented in Figure 2. The pseudowollastonite intensity in Figure 3a drops as P_{CO_2} increases as more carbonate is formed. The ratio between the intensities of calcium carbonate polymorphs changed with P_{CO_2}; aragonite was the main polymorph formed across all pressures, with the calcite intensity increasing with P_{CO_2}. Calcium carbonate formation was also found to increase with the NaOH concentration. Interestingly, the wollastonite intensity in Figure 3a does not decrease with P_{CO_2}, supporting the observation that CO_2 preferentially reacts with pseudowollastonite seen by Plattenberger. At P_{CO_2} = 3 psi, the reaction produced small amounts of tobermorite−13 Å and rhodesite along with gismondine-Na. At 6 psi, the crystalline hydrate produced was mordenite, another sodium aluminum silicate phase likely formed from the borosilicate glass dissolution introducing aluminum. Aragonite and calcite dominated the XRD patterns, with no CCSH phases present in Figure 3a. Similarly, only aragonite and calcite were found at 15 psi. When CCSH phases were not formed at higher P_{CO_2}, the supernatants were visually supersaturated with amorphous silica, increasing with the NaOH concentration. The added CO_2 is expected to have reacted with all of the available calcium, leaving the remaining silica partially suspended in the NaOH solution. The small, broad peak found centered around 2θ = 21° corresponds to the amorphous silica found in the reaction products.

DTG data shown in Figure 3b support the observation that carbonate precipitation dominates over CCSH precipitation at higher P_{CO_2} levels. All conditions have some structural water linked to CSH gel below 100 °C, but only those experiments conducted at 3 psi show evidence of a CCSH dehydration peak. The peak at 90 °C seen in the DTG data of the 15 psi precipitates is expected to be primarily amorphous silica. It should be noted, however, that the dehydration of amorphous calcium carbonate (ACC) could also be contributing to the DTG peaks below 300 °C.[17,44,45] ACC has been observed during carbonation of wollastonite[44] and can concentrate in silica gel.[46] Interestingly, the total amount of crystalline $CaCO_3$ in the precipitates does not increase proportionally with P_{CO_2} in Figure 3b. The 6 psi precipitates were found to contain about 21.3% $CaCO_3$ by mass, and the 3 psi precipitates contained about 26.1% $CaCO_3$ by mass. The 15 psi precipitates did produce the highest amount of $CaCO_3$, at 36.4% by mass.

Reactions with Na_2CO_3. Both CCSH phases and calcium carbonates were found in significant quantities in precipitates when Na_2CO_3 was introduced to the system. Tobermorite−13 Å, pectolite, rhodesite, and gismondine-Na were all found in the 1-day, 2 M Na concentration ($[Na^+]_{Total}$) experiments shown in Figure 4a, forming much earlier than those in the 2 M NaOH experiments without CO_2. In the 7-day precipitates, the rhodesite and gismondine-Na intensities were closer to that of tobermorite−13 Å than what was seen in the precipitates from NaOH experiments shown in Figure 2. Pseudowollastonite was consumed to form the CCSH phases and carbonates. No decrease in the wollastonite intensity was observed in the Na_2CO_3 experiments in Figure 4. Instead, there was a slight increase in the wollastonite intensity at 7 days, consistent with observations by Monasterio-Guillot et al.[17] Here, the total CO_2 added from Na_2CO_3 would equate to a P_{CO_2} of approximately 3.8 psi at 150 °C if the CO_2 added were in gaseous form based on the volume of the reaction vessel.

The DTG data in Figure 4b support the observation that CCSH phases form in 1 day, as seen in the XRD data. After 7 days, the precipitates from Na_2CO_3 experiments lost 9% mass to CSH gel and CCSH dehydration, showing a slight decrease in CCSH dehydration compared with the NaOH experiments. ACC is also expected to contribute to the dehydration DTG peaks observed, as seen in the variable P_{CO_2} experiments, although the amount formed is unknown. The DTG data in Figure 4b also show that at 3 days the Na_2CO_3 precipitates produced the most calcium carbonate, accounting for about 11.6% of the total mass. The Na_2CO_3 precipitates overall showed less carbonation than the P_{CO_2} precipitates at similar amounts of CO_2 and $[Na^+]_{Total}$.

The CCSH phases formed in Na_2CO_3 at 1 M $[Na^+]_{Total}$ differ from the 2 M $[Na^+]_{Total}$ samples, unlike the 1 and 2 M NaOH baseline experiments. The 1 M $[Na^+]_{Total}$ and Na_2CO_3 precipitates in Figure 5a produced primarily rhodesite and gismondine-Na precipitates, with neither tobermorite−13 Å nor pectolite identified. Interestingly, the XRD patterns show that the low-angle peak at 2θ = 7.4° for rhodesite is the highest-intensity peak, whereas prior patterns show the primary peak at 2θ = 13.5°. Pseudowollastonite decreases and wollastonite increases with time in the 1 M $[Na^+]_{Total}$ and Na_2CO_3 precipitates, similar to the 2 M $[Na^+]_{Total}$ and Na_2CO_3 precipitates.

The DTG data in Figure 5b support the trends seen in XRD. The peak at 90 °C is expected to be dehydration of gismondine-

https://doi.org/10.1021/acssuschemeng.3c05110
ACS Sustainable Chem. Eng. 2024, 12, 1844−1856

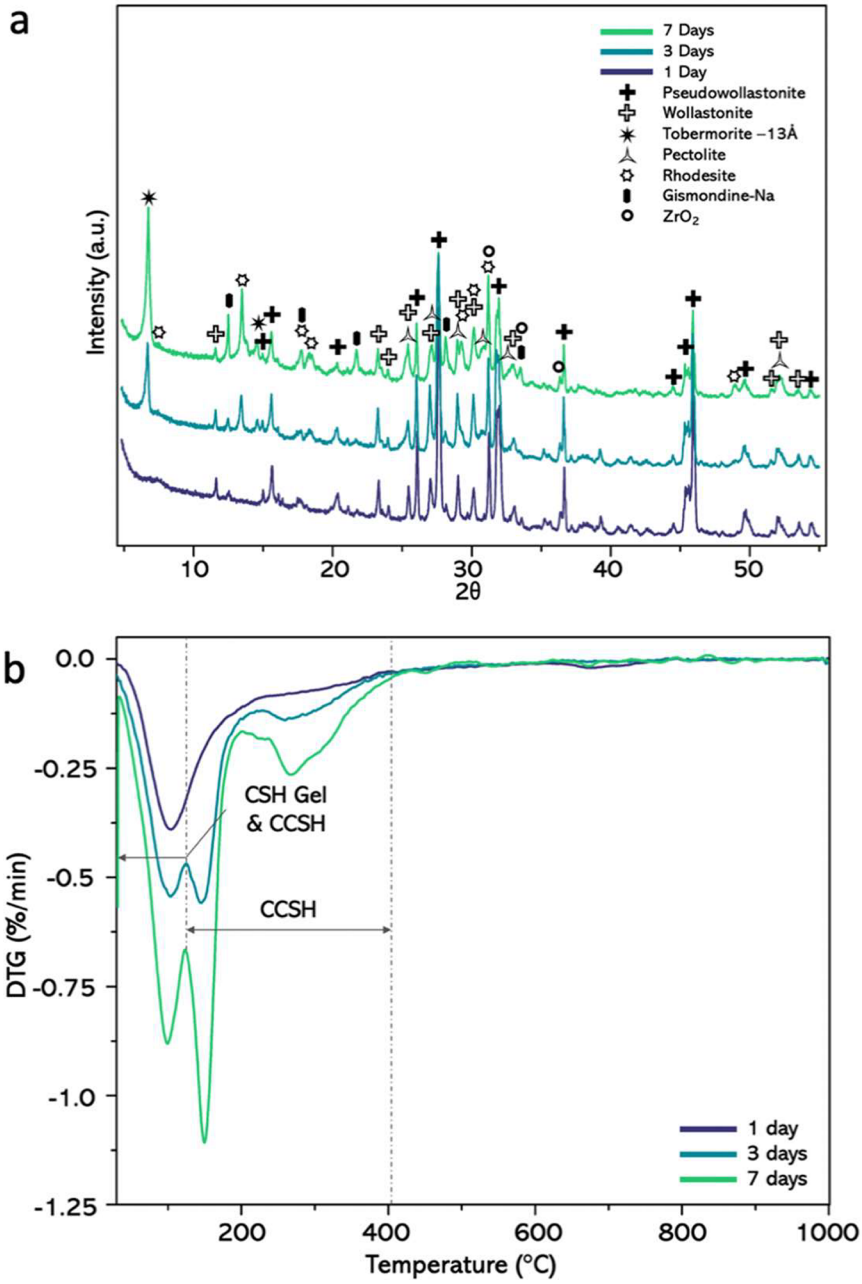

Figure 2. (a) XRD and (b) DTG data from pseudowollastonite and 2 M NaOH recorded by reacting at 150 °C for 1, 3, and 7 days. This figure demonstrates the positive relationship between high [NaOH] and CCSH precipitation from pseudowollastonite over time. The intensities of the CCSH phases increase with time, and the intensities of pseudowollastonite and wollastonite decrease with time. The increased DTG peaks in part b correspond to increasing amounts of CCSH formed.

Na and the CSH gel. No tobermorite dehydration peak is observed at 150 °C. The earlier assumption that rhodesite has a dehydration peak at 250 °C is supported by the prominent peak found in Figure 5b because rhodesite was the dominant CCSH phase in the XRD data. ACC dehydration is expected to contribute to the DTG peaks from 90 to 250 °C, the TG data indicate that, after 7 days, 5.13% of the precipitate mass was lost to water vapor, and the calculated mass of $CaCO_3$ was 7.3%.

Reactions with Al_2O_3. The addition of Al_2O_3 to pseudowollastonite impacted CCSH precipitation, and the effect was most noticeable for the gas-phase CO_2 and NaOH experiments, as shown in Figure 6. In Figure 6a, tobermorite−13 Å is present at 3 psi but at a lower intensity than that seen in the pseudowollastonite experiments without Al_2O_3 in Figure 3a. Additionally, instead of rhodesite, an CCSH phase with no mineral name was matched. The addition of Al_2O_3 also allowed CCSH to precipitate at 6 psi, differing from the precipitates from experiments with pseudowollastonite alone in Figure 3a. Finally, calcite has an increased intensity at 15 psi compared with that in Figure 3a. Similar observations are drawn from the DTG data in Figure 6b. Both the 3 and 6 psi precipitates show minor dehydration peaks indicative of CCSH. An increase in the $CaCO_3$ mass was observed with the addition of Al_2O_3 at 6 and 15 psi compared to Figure 3, while a decrease is seen at 3 psi. Al_2O_3 had only minor effects on the precipitates from the NaOH experiments without CO_2.

The results of comparing the effects of Al_2O_3 to the Na_2CO_3 experiments after 7 days are shown in Figure 7. The

https://doi.org/10.1021/acssuschemeng.3c05110
ACS Sustainable Chem. Eng. 2024, 12, 1844−1856

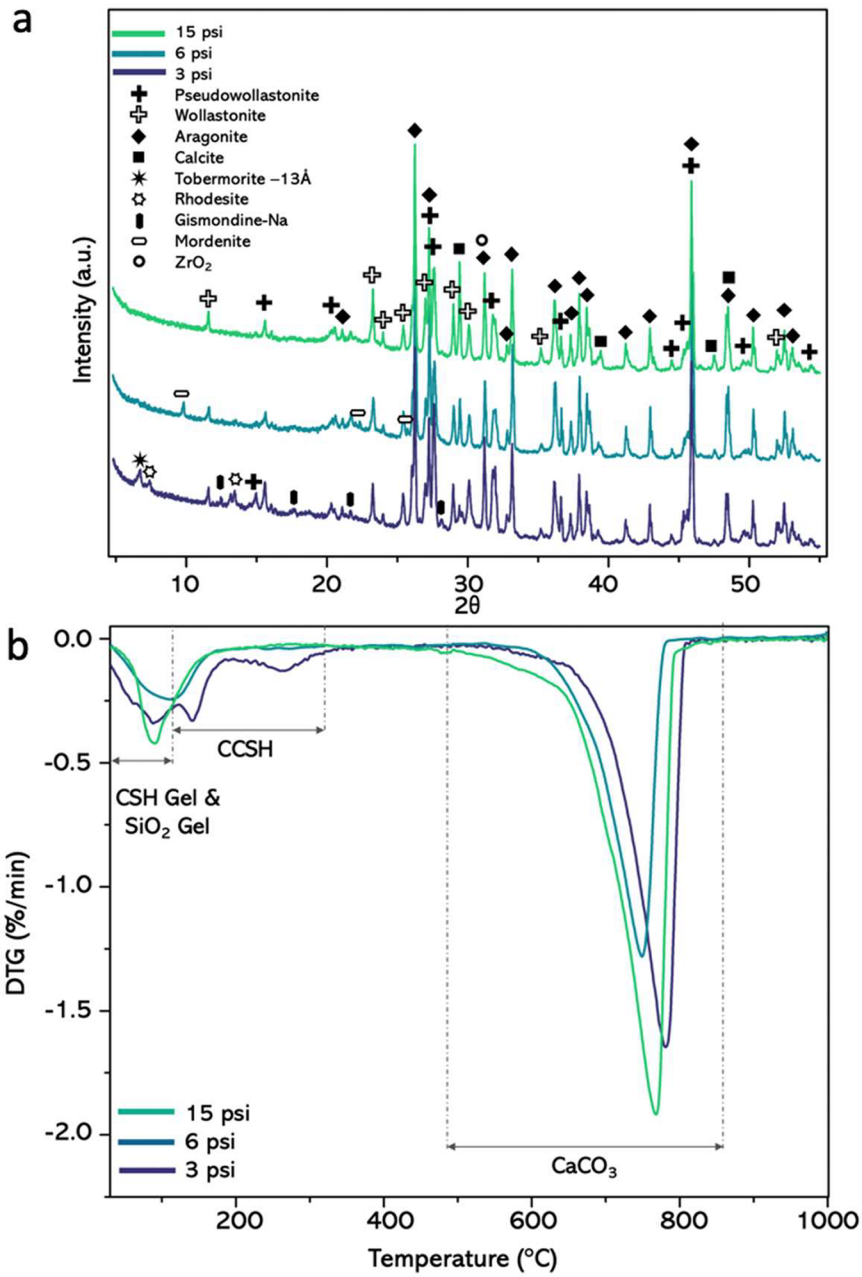

Figure 3. (a) XRD and (b) DTG plots of 2 M NaOH precipitates cured for 7 days at 3, 6, and 15 psi of CO_2. These demonstrate the negative relationship between the CCSH precipitation and P_{CO_2}. Note the low intensities of the CCSH phases at 3 psi (at $2\theta = 7°$) and the absence of a CCSH peak at higher partial pressures of CO_2. The broad peak at $2\theta = 21°$ is attributed to amorphous silica. Part b shows a clear increase in the calcite intensity and a decrease in the CCSH intensity with P_{CO_2}.

tobermorite−13 Å and wollastonite intensities increased with the presence of Al_2O_3, and gismondine-Na decreased in intensity, as seen in Figure 7a. The DTG data in Figure 7b show that Al_2O_3 decreased the dehydration observed but increased carbonation.

Borosilicate Glass Dissolution. The borosilicate test tube chemical composition was found to be $Ca_{0.2}K_{3.8}Na_{8.4}Al_{8.6}B_9Si_{78.8}$ in cation atom percentage, excluding oxygen, as measured via ICP-OES of shards dissolved in a HF and HNO_3 solution. The elemental concentrations from the 7-day-cured NaOH and borosilicate glass experiments without reactants presented in Figure 8 confirm that B, K, Na, and Si are all added to the solution as dissolution products. Similar concentrations were observed at 1 and 3 days. Here, Al and Ca are not shown because their concentrations remained undetectable. All four remaining elements show an increase in concentration with time in the 2 M NaOH experiments while remaining at the same level in the 1 M experiments. Na and Si show similar concentrations, indicating that Na is increasing the Si solubility, likely in the form of colloidal silica. The starting concentration for 1 M NaOH is 40000 ppm, and that for 2 M NaOH is 80000 ppm. The black or gray error bars indicate 1 standard of deviation about the mean, and that very little error was seen for the data collected. The DI water experiments did not have any measurable concentrations of the elements tested and are not included.

https://doi.org/10.1021/acssuschemeng.3c05110
ACS Sustainable Chem. Eng. 2024, 12, 1844−1856

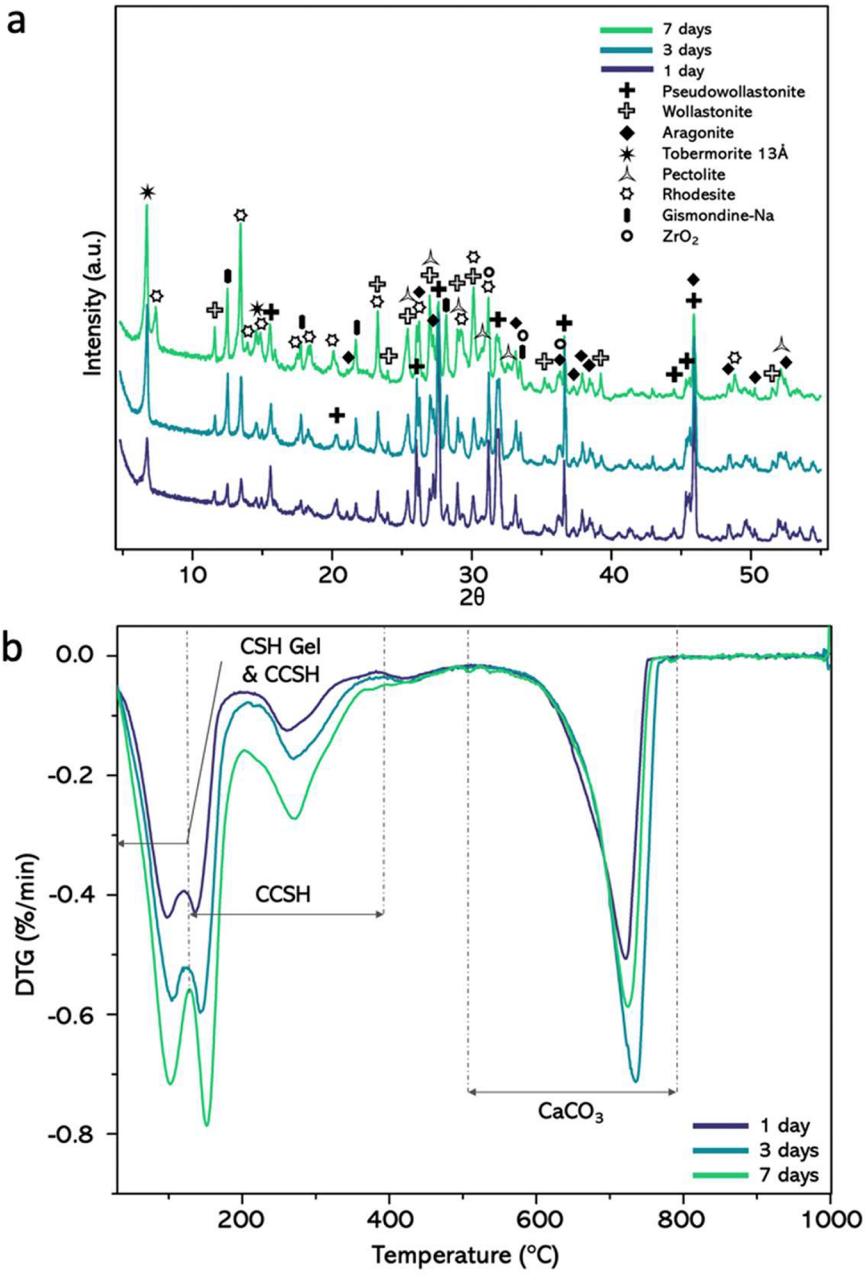

Figure 4. (a) XRD and (b) DTG data of 2 M $[Na^+]_{Total}$ Na_2CO_3 and pseudowollastonite reaction products cured for 1, 3, or 7 days. This figure demonstrates how the use of salt-based CO_2 allows for both CCSH and $CaCO_3$ phases to precipitate. Additionally, these results demonstrate the positive relationship between the CCSH precipitation and $[Na^+]$ in alkaline solutions. In part a, note that tobermorite−13 Å and other CCSH phases precipitated after 1 day. Additionally, note that wollastonite increases in intensity with time, suggesting preferential dissolution of pseudowollastonite.

■ DISCUSSION

The carbonation of calcium silicates under hydrothermal and alkaline conditions is influenced by a complex set of chemical and physical processes that include dissolution and precipitation chemistry, diffusion of CO_2 and other solutes, and the presence of trace chemical species in the aqueous phase. Our experiments reveal four key findings about this system: (1) the coprecipitation of CCSH phases and $CaCO_3$ is possible under the right pH conditions, and it increases with the total $[Na^+]$; (2) using Na_2CO_3 to drive carbonation, instead of $CO_2(g)$, promotes a more balanced precipitation of CCSH and carbonate; (3) trace species, here dissolved from the borosilicate test tubes, can impact CCSH speciation; (4) the addition of Al_2O_3 aids the crystallinity of CCSH phases.

A graphical summary of the three reaction pathways studied here is presented in Figure 9. Reaction 1 shows (a) pseudowollastonite dissolving in NaOH solution, producing Ca^{2+} and colloidal silica, and the borosilicate glass producing colloidal silica, (b) the ordering of colloidal silica in solution, and (c) the precipitation of CCSH phases. Reaction 2 shows (a) gaseous CO_2 forming carbonic acid, which dissolves pseudowollastonite in NaOH, producing Ca^{2+} and colloidal silica, (b) bicarbonate ion interacting with Ca^{2+} ions, and (c) the precipitation of $CaCO_3$ phases and amorphous silica. Reaction 3 shows (a) pseudowollastonite dissolving in Na_2CO_3 solution, producing carbonate ions, Ca^{2+}, and colloidal silica, (b) the precipitation of $CaCO_3$ phases while CO_2 escapes the solution

https://doi.org/10.1021/acssuschemeng.3c05110
ACS Sustainable Chem. Eng. 2024, 12, 1844−1856

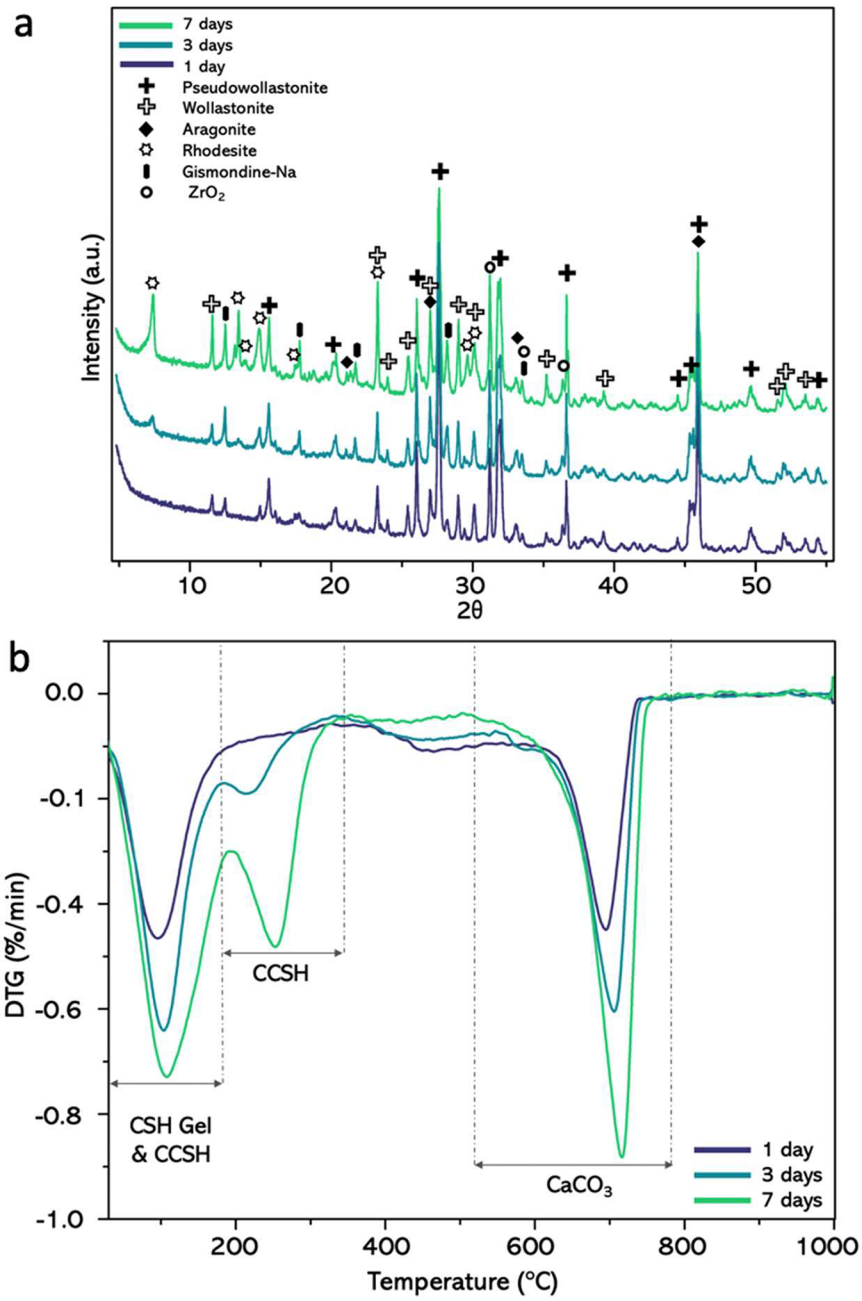

Figure 5. (a) XRD and (b) DTG of the 1 M $[Na^+]_{Total}$ and Na_2CO_3 experiments carried out after 1, 3, and 7 days. Changes in the precipitates identified at lower [Na] from Na_2CO_3 compared to Figure 4. Note the absence of tobermorite−13 Å and pectolite in part a.

and silica colloids order, and (c) the precipitation of CCSH phases.

The precipitation of both CCSH phases and $CaCO_3$ was shown to increase with $[Na^+]$ under the conditions tested. For the CCSH phases, the increase in $[Na^+]$ is believed to boost the dissolution of both pseudowollastonite and borosilicate glass by slowly hydrolyzing silica along the exposed surfaces,[47−49] notionally described in eq 1.

$$x\mathrm{SiO_2(am)} + \mathrm{H_2O(l)} + \mathrm{OH^-} \xleftrightarrow{\mathrm{Na^+}} \mathrm{Si}_x\mathrm{O}_y(\mathrm{OH})^{\delta}(\mathrm{aq}) \quad (1)$$

The δ indicates the variable charges of the different forms of aqueous silica. Silica enters the solution and is then expected to polymerize and form semiordered structures with the aid of Na^+.[48] The silica structures then react with aqueous Ca to form either the CSH gel or the CCSH phases identified. From the data collected here, we cannot infer whether crystallization of CSH gel or direct precipitation from solution is the dominant pathway to form CCSH phases. However, we suspect that reactions between colloidal silica and Ca^{2+} ions do drive precipitation because significantly less precipitation was reported by Monasterio-Guillot under similar curing conditions using NaOH-inert Teflon vessels. The increase in NaOH is expected to increase $CaCO_3$ precipitation by improving the gas solubility of CO_2 at temperature. The gas phase CO_2 enters the solution via

$$\mathrm{CO_2(g)} + \mathrm{H_2O(aq)} \leftrightarrow \mathrm{H_2CO_3(aq)} \leftrightarrow \mathrm{H^+(aq)} + \mathrm{HCO_3^-(aq)} \leftrightarrow 2\mathrm{H^+(aq)} + \mathrm{CO_3^{2-}(aq)} \quad (2)$$

https://doi.org/10.1021/acssuschemeng.3c05110
ACS Sustainable Chem. Eng. 2024, 12, 1844−1856

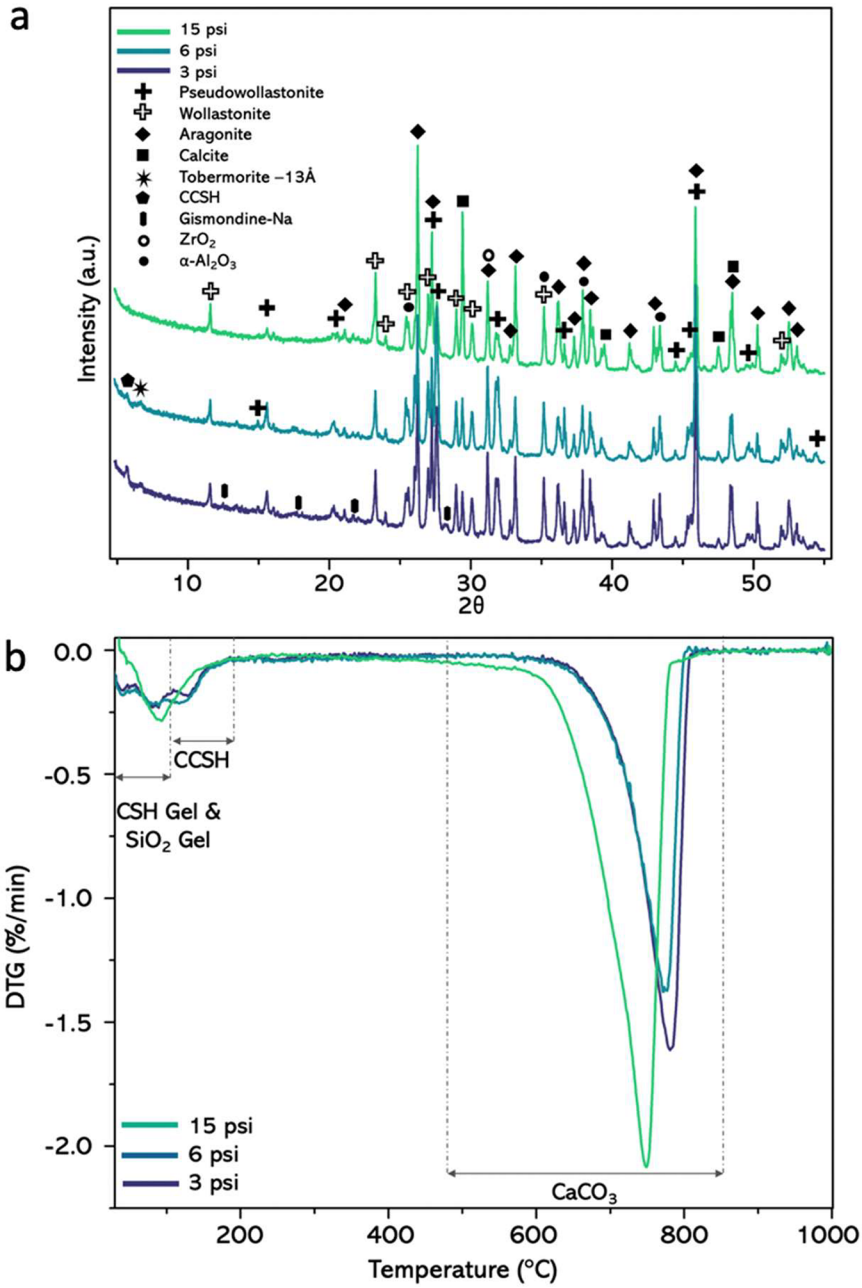

Figure 6. (a) XRD and (b) DTG data from pseudowollastonite, Al_2O_3, and 2 M NaOH cured in 3, 6, or 15 psi at 150 °C for 1, 3, and 7 days. The data show how the presence of Al_2O_3 changed the CCSH phases and the maximum P_{CO_2} at which they precipitate compared to those in Figure 3.

H^+ then dissolves pseudowollastonite into aqueous silica and Ca^{2+}, the latter of which reacts readily with CO_3^{2-} in the solution to form calcium carbonates.

Increasing P_{CO_2} led to calcium carbonate becoming the dominant precipitate. This could be because the polymerization of aqueous SiO_2 is sluggish, and so the calcium is consumed to form calcium carbonates, which prevents CCSH precipitation. Additionally, the aqueous carbonate species acted as acids to buffer the NaOH solution, as shown in eq 2. The reduced pH could also lower the favorability of CCSH precipitation. At lower P_{CO_2}, the push toward calcium carbonates and pH changes is less intense, allowing for small amounts of CCSH to precipitate, as seen in Figure 3a at 3 psi.

The pseudowollastonite and Na_2CO_3 experiments precipitated both calcium carbonates and CCSH phases, with molar concentrations of Na and CO_2 similar to those of some of the P_{CO_2} experiments. Equation 2 proceeds in reverse when Na_2CO_3 dissociates into Na^+ and CO_3^{2-}, as described in eqs 3 and 4.

$$Na_2CO_3(s) \leftrightarrow 2Na^+(aq) + CO_3^{2-}(aq) \tag{3}$$

$$\begin{aligned} CO_3^{2-}(aq) + 2H_2O(l) &\leftrightarrow HCO_3^-(aq) + OH^-(aq) + H_2O(l) \\ &\leftrightarrow H_2CO_3(aq) + 2OH^-(aq) \\ &\leftrightarrow CO_2(g) + H_2O(l) + 2OH^-(aq) \end{aligned} \tag{4}$$

Equation 4 is driven to the right as large concentrations of CO_3^{2-} enter the solution when the salt dissolves. While H_2CO_3 and HCO_3^- ions do form and attack pseudowollastonite to form

https://doi.org/10.1021/acssuschemeng.3c05110
ACS Sustainable Chem. Eng. 2024, 12, 1844−1856

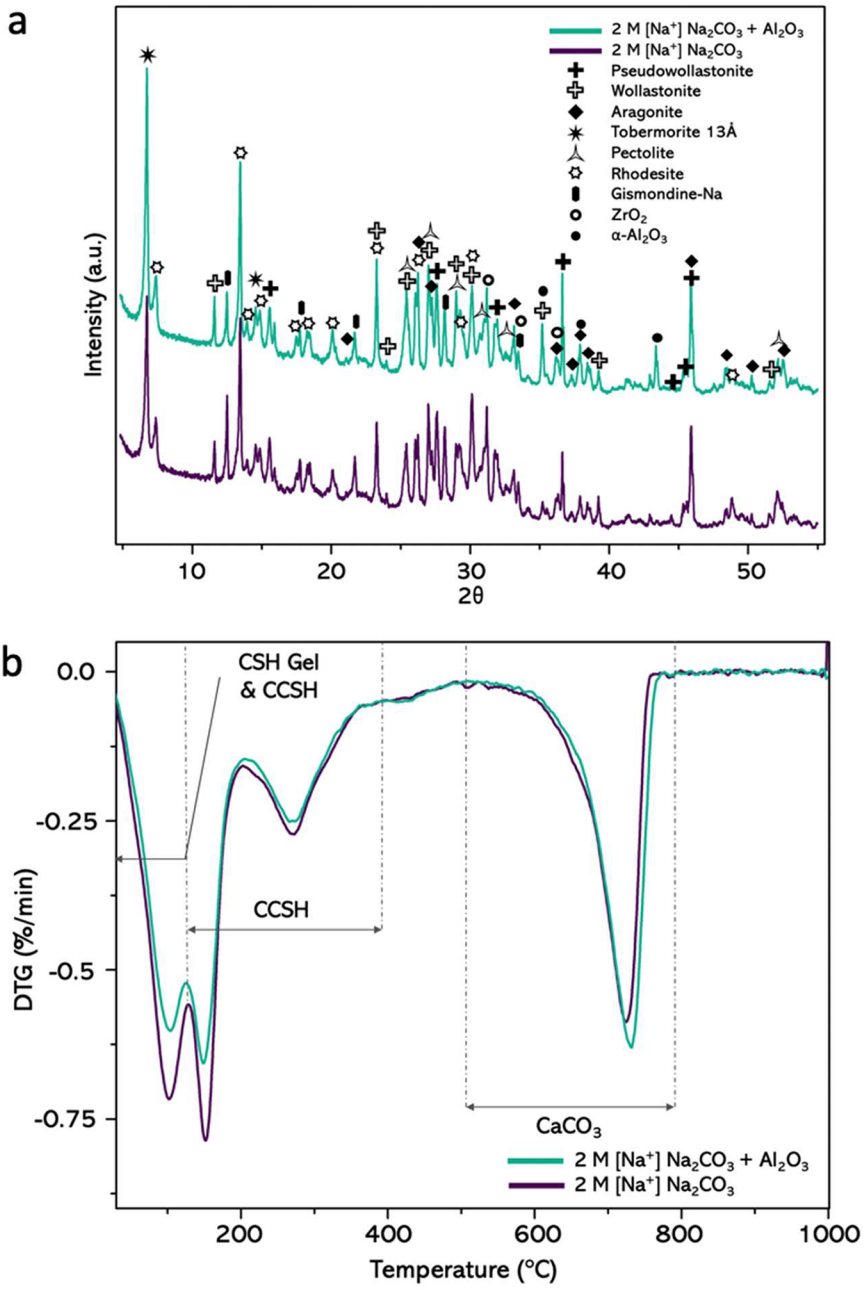

Figure 7. (a) XRD and (b) DTG data of 2 M [Na^+] and Na_2O_3 precipitates from pseudowollastonite mixed with and without Al_2O_3 cured for 7 days. This figure illustrates how the presence of Al_2O_3 increased the intensity of tobermorite−13 Å but decreased the total hydration. Note the difference in the intensities of tobermorite−13 Å, gismondine-Na, and wollastonite. Also note the changes in the dehydration peaks in the DTG data in part b.

calcium carbonates, the reaction is driven to produce CO_2. The aqueous CO_2 is expected to escape from the solution into the undersaturated headspace in gaseous form to equilibrate. The water−CO_2 reaction to form H_2CO_3 in eq 2 is expected to be the rate-limiting step of the carbonate buffer reaction. Additionally, the aqueous carbonate species acts as a base, maintaining a favorable pH for CCSH precipitation. With less CO_2 consuming Ca^{2+} and desirable pH levels, aqueous silica may react with Ca^{2+} to form CCSH phases.

The borosilicate glass test tubes used here impacted the precipitation of CCSH phases. Rhodesite and gismondine-Na were identified and likely formed with K^+ and Al^{3+} from the dissolving glass. The aqueous silica and dissolution species may have also improved the precipitation rate of tobermorite−13 Å.

The addition of Al_2O_3 was shown to increase the amount of $CaCO_3$ precipitated after 3 days of curing pseudowollastonite either in gaseous CO_2 or in Na_2CO_3 solution. Al_2O_3 also extended the P_{CO_2} range in which the CCSH phase precipitated from pseudowollastonite, as seen in Figure 6. Figure 7 shows that Al_2O_3 improved the crystallinity of CCSH phases precipitated from Na_2CO_3, while also decreasing the total amount of hydrates formed when pseudowollastonite was cured in the presence of CO_2. However, similar effects were not seen in the precipitates from the NaOH experiments, which showed similar intensities and total hydration. Overall, the effect of aluminum on CCSH speciation needs to be better understood given how common a trace element it is in many calcium silicate feedstocks.

https://doi.org/10.1021/acssuschemeng.3c05110
ACS Sustainable Chem. Eng. 2024, 12, 1844−1856

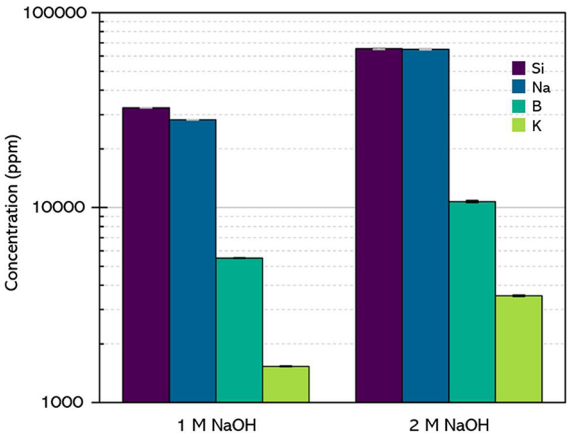

Figure 8. Logarithmic plot of the elemental concentrations from the powderless borosilicate glass experiment supernatants after 7 days of curing, measured via ICP-OES. The data highlight that the glass dissolution contributed significant amounts of aqueous Si to the solution during curing, which, in turn, allowed for the diversity of CCSH phases identified in the experiments without gaseous CO_2.

CONCLUSIONS

The formation of CCSH such as tobermorite and carbonates from a model monocalcium silicate under carbonation conditions was found to be influenced by the NaOH concentration, the partial pressure of CO_2, and the use of Na_2CO_3 as a source of both Na^+ and CO_2. NaOH was found to improve both CCSH and calcium carbonate precipitation. The use of gas phase CO_2 enhanced the formation of calcium carbonates, even at a low P_{CO_2}. In contrast, the use of Na_2CO_3 was found to produce significant amounts of both CCSH phases and calcium carbonates. This is important because it suggests that carbonating concretes with Na_2CO_3 instead of gas phase CO_2 could produce mortars and concretes with some of the desirable mechanical properties of ancient Roman cements that are rich in CCSH phases. The use of Na_2CO_3 at standard pressures could also potentially simplify the curing of alternative low carbon concretes.

AUTHOR INFORMATION

Corresponding Author

Andres F. Clarens − *Department of Civil and Environmental Engineering, University of Virginia, Charlottesville, Virginia 22904, United States*; orcid.org/0000-0002-0606-9717; Email: andres@virginia.edu

Authors

Coleman Tolliver − *Department of Materials Science and Engineering, University of Virginia, Charlottesville, Virginia 22904, United States*

Suzanne Nguyen − *Department of Civil and Environmental Engineering, University of Virginia, Charlottesville, Virginia 22904, United States*

Kimmie Dela Cerna − *Department of Civil and Environmental Engineering, University of Virginia, Charlottesville, Virginia 22904, United States*

Rachel McNamara − *Department of Materials Science and Engineering, University of Virginia, Charlottesville, Virginia 22904, United States*

Elizabeth J. Opila − *Department of Materials Science and Engineering, University of Virginia, Charlottesville, Virginia 22904, United States*

Complete contact information is available at: https://pubs.acs.org/10.1021/acssuschemeng.3c05110

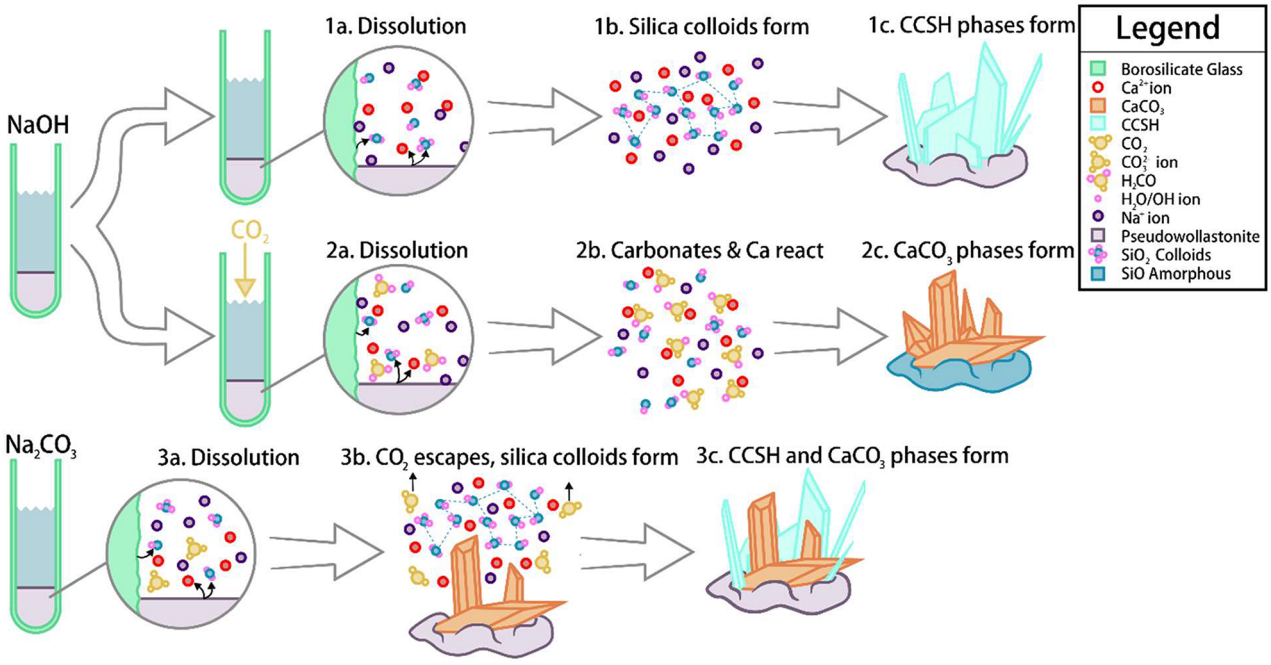

Figure 9. Schematic outlining the precipitation pathways under the conditions explored in this work. The abbreviated reactions depicted are as follows: (1) pseudowollastonite dissolved in a NaOH solution to precipitate CCSH phases; (2) pseudowollastonite dissolved from carbonic acid produced from gaseous CO_2 and precipitating $CaCO_3$ phases; (3) pseudowollastonite dissolved in a Na_2CO_3 solution and precipitating both $CaCO_3$ and CCSH phases.

https://doi.org/10.1021/acssuschemeng.3c05110
ACS Sustainable Chem. Eng. 2024, 12, 1844−1856

Notes

The authors declare no competing financial interest.

■ ACKNOWLEDGMENTS

The authors acknowledge financial support from the U.S. Department of Energy Advanced Research Projects for Energy agency via Grant DE-AR0001858 and the U.S. National Science Foundation via Grant 2234543.

■ REFERENCES

(1) Ellis, L. D.; Badel, A. F.; Chiang, M. L.; Park, R. J. Y.; Chiang, Y. M. Toward electrochemical synthesis of cement—An electrolyzer-based process for decarbonating CaCO3 while producing useful gas streams. *Proc. Natl. Acad. Sci. U. S. A.* **2020**, *117*, 12584−12591.

(2) Golewski, G. L. Green concrete based on quaternary binders with significant reduced of co2 emissions. *Energies* **2021**, *14*, 4558.

(3) USGS Mineral Commodities Summary. 2022.

(4) Awoyera, P.; Adesina, A. Correction to: Durability Properties of Alkali Activated Slag Composites: Short Overview (Silicon, (2020), 12, 4, (987−996), 10.1007/s12633−019−00199−1). *Silicon* **2020**, *12*, 1511.

(5) U.S. Geological Survey. *Mineral Commodoty Summaries* **2020**, 86−87.

(6) Mendes, A.; Sanjayan, J.; Collins, F. Phase transformations and mechanical strength of OPC/Slag pastes submitted to high temperatures. *Mater. Struct. Constr.* **2008**, *41*, 345−350.

(7) Sajedi, F.; Razak, H. A. Comparison of different methods for activation of ordinary Portland cement-slag mortars. *Constr. Build. Mater.* **2011**, *25*, 30−38.

(8) Golewski, G. L. The Effect of the Addition of Coal Fly Ash (CFA) on the Control of Water Movement within the Structure of the Concrete. *Materials (Basel)* **2023**, *16*, 5218.

(9) Golewski, G. L. Combined Effect of Coal Fly Ash (CFA) and Nanosilica (nS) on the Strength Parameters and Microstructural Properties of Eco-Friendly Concrete. *Energies* **2023**, *16*, 452.

(10) Amran, M.; et al. Slag uses in making an ecofriendly and sustainable concrete: A review. *Constr. Build. Mater.* **2021**, *272*, No. 121942.

(11) Pacheco-Torgal, F. Introduction to Handbook of Alkali-Activated Cements, Mortars and Concretes. *Handbook of Alkali-Activated Cements, Mortars and Concretes*; Woodhead Publishing Limited, 2015. DOI: 10.1533/9781782422884.1.

(12) Juenger, M. C. G.; Winnefeld, F.; Provis, J. L.; Ideker, J. H. Advances in alternative cementitious binders. *Cem. Concr. Res.* **2011**, *41*, 1232−1243.

(13) Awoyera, P.; Adesina, A. A critical review on application of alkali activated slag as a sustainable composite binder. *Case Stud. Constr. Mater.* **2019**, *11*, No. e00268.

(14) Plattenberger, D. A.; Ling, F. T.; Tao, Z.; Peters, C. A.; Clarens, A. F. Calcium Silicate Crystal Structure Impacts Reactivity with CO2 and Precipitate Chemistry. *Environ. Sci. Technol. Lett.* **2018**, *5*, 558−563.

(15) Plattenberger, D. A.; Opila, E. J.; Shahsavari, R.; Clarens, A. F. Feasibility of Using Calcium Silicate Carbonation to Synthesize High-Performance and Low-Carbon Cements. *ACS Sustain. Chem. Eng.* **2020**, *8*, 5431−5436.

(16) Plattenberger, D. A.; Ling, F. T.; Peters, C. A.; Clarens, A. F. Targeted Permeability Control in the Subsurface via Calcium Silicate Carbonation. *Environ. Sci. Technol. Lett.* **2019**, *53*, 7136.

(17) Monasterio-Guillot, L.; Di Lorenzo, F.; Ruiz-Agudo, E.; Rodriguez-Navarro, C. Reaction of pseudowollastonite with carbonate-bearing fluids: Implications for CO2 mineral sequestration. *Chem. Geol.* **2019**, *524*, 158−173.

(18) Komarneni, S.; Roy, D. M. *Tobermorites: A New Family of Cation Exchangers* **1983**, *221*, 647−648.

(19) Jackson, M. D.; et al. Unlocking the secrets of Al-tobermorite in Roman seawater concrete. *Am. Mineral.* **2013**, *98*, 1669−1687.

(20) Jackson, M. D.; et al. Phillipsite and Al-tobermorite mineral cements produced through low-temperature water-rock reactions in Roman marine concrete. *Am. Mineral.* **2017**, *102*, 1435−1450.

(21) Jackson, M. D.; et al. Extreme durability in ancient Roman concretes. *Am. Ceram. Soc. Bull.* **2018**, *97*, 22−28.

(22) Jackson, M. D.; Moon, J.; Gotti, E.; Taylor, R.; Chae, S. R.; Kunz, M.; Emwas, A.-H.; Meral, C.; Guttmann, P.; Levitz, P.; Wenk, H.-R.; Monteiro, P. J. M.; et al. Material and Elastic Properties of Al-Tobermorite in Ancient Roman Seawater Concrete. *J. Am. Ceram. Soc.* **2013**, *96*, 2598−2606.

(23) Guo, X.; Meng, F.; Shi, H. Microstructure and characterization of hydrothermal synthesis of Al-substituted tobermorite. *Constr. Build. Mater.* **2017**, *133*, 253−260.

(24) Galvánková, L.; MáSilko, J.; Solný, T.; Štěpánková, E. Tobermorite Synthesis under Hydrothermal Conditions. *Procedia Eng.* **2016**, *151*, 100−107.

(25) Gabrovsek, R.; Kurbus, B.; Muller, D.; Wieker, W. Tobermorite formation in the system CaO, C3S-SiO2-Al2O3-NaOH-H2O under hydrothermal conditions. *Cem. Concr. Res.* **1993**, *23*, 321−328.

(26) Houston, J. R.; Maxwell, R. S.; Carroll, S. A. Transformation of meta-stable calcium silicate hydrates to tobermorite: Reaction kinetics and molecular structure from XRD and NMR spectroscopy. *Geochem. Trans.* **2009**, *10*, 1−14.

(27) Maeda, H.; Abe, K.; Ishida, E. H. Hydrothermal synthesis of aluminum substituted tobermorite by using various crystal phases of alumina. *J. Ceram. Soc. Japan* **2011**, *119*, 375−377.

(28) Matekonis, G.; Šiaučiunas, R.; Vaičiukyniene, D. Hydrothermal synthesis and characterization of Na^+ and $[Al^{3+} + Na^+]$-substituted tobermorite in $CaO-SiO_2 \cdot nH_2O-H_2O$ System. *Medziagotyra* **2010**, *16*, 242−248.

(29) Shaw, S.; Clark, S. M.; Henderson, C. M. B. Hydrothermal formation of the calcium silicate hydrates, tobermorite (Ca5Si6O16-(OH)2 · 4H2O) and Xonotlite (Ca6Si6O17(OH)2): An in situ synchrotron study. *Chem. Geol.* **2000**, *167*, 129−140.

(30) Siauciunas, R.; Janickis, V.; Palubinskaite, D.; Ivanauskas, R. The sorption properties of tobermorite modified with Na^+ and Al^{3+} ions. *Ceramics-Silikáty* **2004**, *48*, 76−82.

(31) Komarneni, S.; Breval, E.; Miyake, M.; Roy, R. Cation-exchange properties of (Al + Na)-substituted synthetic tobermorites. *Clays Clay Miner.* **1987**, *35*, 385−390.

(32) Mitsuda, T.; Taylor, H. F. Influence of Aluminum on the conversion of calcium silicate hydrate gels into 11 Å tobermorite at 90°C and 120°C. *Cem. Concr. Res.* **1975**, *5*, 203−210.

(33) Cao, P.; Li, G.; Luo, J.; Rao, M.; Jiang, H.; Peng, Z.; Jiang, T.; et al. Alkali-reinforced hydrothermal synthesis of lathy tobermorite fibers using mixture of coal fly ash and lime. *Constr. Build. Mater. J.* **2020**, *238*, 117655.

(34) Wu, Y.; Pan, X.; Li, Q.; Yu, H. Crystallization and phase transition of tobermorite synthesized by hydrothermal reaction from dicalcium silicate. *Int. J. Appl. Ceram. Technol.* **2020**, *17*, 1213−1223.

(35) Coleman, N. J.; Brassington, D. S. Synthesis of Al-substituted 11 Å tobermorite from newsprint recycling residue: A feasibility study. *Mater. Res. Bull.* **2003**, *38*, 485−497.

(36) Youssef, H.; Ibrahim, D.; Komarneni, S.; Mackenzie, K. J. D. Synthesis of 11 Å Al-substituted tobermorite from trachyte rock by hydrothermal treatment. *Ceram. Int.* **2010**, *36*, 203−209.

(37) Casey, W. H. Dynamics and durability. *Rev. Mod. Phys.* **2008**, *7*, 930−932.

(38) Yang, H.; Prewitt, C. T. On the crystal structure of pseudowollastonite (CaSiO3). *Am. Mineral.* **1999**, *84*, 929−932.

(39) Toby, B. H.; Von Dreele, R. B. GSAS-II: The genesis of a modern open-source all purpose crystallography software package. *J. Appl. Crystallogr.* **2013**, *46*, 544−549.

(40) Tajuelo Rodriguez, E.; Garbev, K.; Merz, D.; Black, L.; Richardson, I. G. Thermal stability of C-S-H phases and applicability of Richardson and Groves' and Richardson C-(A)-S-H(I) models to synthetic C-S-H. *Cem. Concr. Res.* **2017**, *93*, 45−56.

(41) Beaudoin, J. J.; Sato, T.; Tumidajski, P. J. The Thermal decomposit ion of $Ca(OH)_2$ polymorphs. *NRC Publications Archive*; RILEM Publication, 2006; Vol. *2*, pp 1−15.
(42) Galan, I.; Glasser, F. P.; Andrade, C. Calcium carbonate decomposition. *J. Therm. Anal. Calorim.* **2013**, *111*, 1197−1202.
(43) Farmer, V. C.; Jeevaratnam, J.; Speakmann, K.; Taylor, H. F. W. Thermal decomposition of 14 Å Tobermorite from Crestmore. *Symposium on Structure of Portland Cement Paste and Concrete*; Spec. Rep. 90; U.S. Highway Res. Board, Washington, 1966; Vol. *90*, pp 291−299.
(44) Miller, Q. R. S.; et al. Insights into silicate carbonation processes in water-bearing supercritical CO2 fluids. *Int. J. Greenh. Gas Control* **2013**, *15*, 104−118.
(45) Ihli, J.; Wong, W. C.; Noel, E. H.; Kim, Y.-Y.; Kulak, A. N.; Christenson, H. K.; Duer, M. J.; Meldrum, F. C.; et al. Dehydration and crystallization of amorphous calcium carbonate in solution and in air. *Nat. Commun.* **2014**, *5*, 1−10.
(46) Ashraf, W. Reaction kinetics, microstructural features and mechanical properties of CO_2 activated low-lime calcium silicate binders. Dissertation, Purdue University, West Lafayette, IN, 2017.
(47) Warring, S. L.; Beattie, D. A.; McQuillan, A. J. Surficial Siloxane-to-Silanol Interconversion during Room-Temperature Hydration/Dehydration of Amorphous Silica Films Observed by ATR-IR and TIR-Raman Spectroscopy. *Langmuir* **2016**, *32*, 1568−1576.
(48) Rimsza, J. M.; Jones, R. E.; Criscenti, L. J. Interaction of NaOH solutions with silica surfaces. *J. Colloid Interface Sci.* **2018**, *516*, 128−137.
(49) Manikandan, S.; Jagannath; Shrikhande, V. K.; Kothiyal, G. P. Degradation behaviour of borosilicate glass: Some studies. *Anti-Corrosion Methods Mater.* **2006**, *53*, 303−309.

https://doi.org/10.1021/acssuschemeng.3c05110
ACS Sustainable Chem. Eng. 2024, 12, 1844−1856